Inorg. Chem. **2006**, *45*, 722–731

Large Gas–Solid Structural Differences in Complexes of Haloacetonitriles with Boron Trifluoride

James A. Phillips,*,† Jason A. Halfen,*,† John P. Wrass,† Christopher C. Knutson,† and Christopher J. Cramer‡

Department of Chemistry, University of Wisconsin−Eau Claire, 105 Garfield Avenue, Eau Claire, Wisconsin 54701, and Department of Chemistry and Supercomputer Institute, University of Minnesota, 207 Pleasant Street SE, Minneapolis, Minnesota 54455

Received September 1, 2005

The structural properties of the singly halogenated derivatives of $CH_3CN–BF_3$ (X–$CH_2CN–BF_3$: X = F, Cl, Br, I) have been investigated via single-crystal X-ray crystallography, solid-state infrared spectroscopy, and correlated electronic–structure theory. Taken together, these data illustrate large differences between the gas-phase and solid-state structures of these systems. Calculated gas-phase structures (B3PW91/aug-cc-pVTZ) of $FCH_2CN–BF_3$, $ClCH_2CN–BF_3$, and $BrCH_2CN–BF_3$ indicate that the B–N dative bonds in these systems are quite weak, with distances of 2.422, 2.374, and 2.341 Å, respectively. However, these distances, as well as other calculated structural parameters and normal-mode vibrational frequencies, indicate that the dative interactions do become slightly stronger in proceeding from F– to Br–$CH_2CN–BF_3$. In contrast, solid-state structures for $FCH_2CN–BF_3$, $ClCH_2CN–BF_3$, and $ICH_2CN–BF_3$ from X-ray crystallography all have B–N distances that are quite short, about 1.65 Å. Thus, the B–N distances of the F- and Cl-containing derivatives contract by over 0.7 Å upon crystallization. Large shifts in the vibrational modes involving motions of the BF_3 subunit parallel these structural changes. An X-ray crystal structure could not be determined for $BrCH_2CN–BF_3$(s), but the solid-state IR spectrum is consistent with those obtained previously for related complexes and suggests that the solid-state structure resembles those of the others, and in turn, implicates a large gas–solid structural difference for this species as well.

I. Introduction

The structure and bonding of nitrile−boron trifluoride complexes has been the subject of numerous studies.[1−23] Most of these have focused upon $CH_3CN−BF_3$[1−13] and/or $HCN−BF_3$,[1−2,8−9,13−22] and recent interest has stemmed from the fact that the gas-phase structures of these species manifest partial bonds, which seem to defy classification as purely bonding or nonbonding interactions.[1,2] For example, $CH_3CN−$

* To whom correspondence should be addressed. Phone: 715-836-5399 (J.A.P.); 715-836-4360 (J.A.H.). Fax: 715-836-4979 (J.A.P.); 715-836-4979 (J.A.H.). E-mail: phillija@uwec.edu (J.A.P.); halfenja@uwec.edu (J.A.H.).
† University of Wisconsin−Eau Claire.
‡ University of Minnesota.

(1) Leopold, K. R., Canagaratna, M.; Phillips, J. A. *Acc. Chem. Res.* **1997**, *30*, 57.
(2) Leopold, K. R. In *Advances in Molecular Structure Research*; Hargittai, M., Hargittai, I., Eds.; JAI Press: Greenwich, CT, 1996; Vol. 2.
(3) Dvorak, M. A.; Ford, R. S.; Suenram, R. D.; Lovas, F. J.; Leopold, K. R. *J. Am. Chem. Soc.* **1992**, *114*, 108.
(4) Swanson, B.; Shriver, D. F.; Ibers, J. A. *Inorg. Chem.* **1969**, *8*, 2183.
(5) (a) Purcell, K. F.; Drago, R. S. *J. Am. Chem. Soc.* **1966**, *88*, 919. (b) Coerver, H. J.; Curran, C. *J. Am. Chem. Soc.* **1958**, *80*, 3522.
(6) Swanson, B.; Shriver, D. F. *Inorg. Chem.* **1970**, *6*, 1406.
(7) Jurgens, R.; Almlöf, J. *Chem. Phys. Lett.* **1991**, *176*, 263.
(8) Jiao, H. J.; Schleyer, P. v. R. *J. Am. Chem. Soc.* **1994**, *116*, 7429.
(9) Jonas, V.; Frenking, G.; Reetz, M. T. *J. Am. Chem. Soc.* **1994**, *116*, 8741.
(10) Cho, H-.G.; Cheong, B-.S. *J. Mol. Struct. (THEOCHEM)* **2000**, *496*, 185.
(11) Wells, N. P.; Phillips, J. A. *J. Phys. Chem. A* **2002**, *106*, 1518.
(12) Giesen, D. J.; Phillips, J. A. *J. Phys Chem. A* **2003**, *107*, 4009.
(13) Beattie, I. R.; Jones, P. J. *Angew. Chem., Int. Ed. Engl.* **1996**, *35*, 1527.
(14) Reeve, S. W.; Burns, W. A.; Lovas, F. J.; Suenram, R. D.; Leopold, K. R. *J. Phys. Chem.* **1993**, *97*, 10630.
(15) Burns. W. A.; Leopold, K. R. *J. Am. Chem. Soc.* **1993**, *115*, 11622.
(16) Hankinson, D. J.; Amlôf, J.; Leopold, K. R.; *J. Phys. Chem.* **1996**, *100*, 6904.
(17) Iglesias, E.; Sordo, T. L.; Sordo, J. A. *Chem. Phys. Lett*. **1996**, *248*, 179.
(18) (a) Nxumalo, L. M.; Andrezejak, M.; Ford, T. A. *J. Chem, Info. Comput. Sci.* **1996**, *36*, 377. (b) Nxumalo, L. M.; Andrzejak, M.; Ford, T. A. *Vib. Spectrosc.* **1996**, 12, 221.
(19) Cabaleiro-Lago, E. M.; Ríos, M. A. *Chem Phys. Lett.* **1998**, *294*, 272.
(20) Fiacco, D. L.; Leopold, K. R. *J. Phys. Chem. A* **2003**, *107*, 2808.
(21) Venter, G.; Dillen, J. *J. Phys. Chem. A* **2004**, *108*, 8378.
(22) Phillips, J. A. and Cramer, C. J. *J. Chem. Theor. Comput.* **2005**, *1*, 827.
(23) Phillips, J. A.; Geisen, D. J.; Wells, N. P.; Halfen, J. A.; Knutson C. C.; Wrass, J. P. *J. Phys. Chem. A* **2005**, *109*, 8199.

10.1021/ic051491x CCC: $33.50
Published on Web 12/24/2005

Table 1. Gas Phase Proton Affinities and Ionization Potentials[a]

molecule	ionization potential (eV)	proton affinity (kJ/mol)
NH_3	10.07	853.6
$(CH_3)_3CCN$	−	810.9
$BrCH_2CN$	11.28	−
$ClCH_2CN$	11.95	745.7
CH_3CN	12.20	779.2
FCH_2CN	12.81	−
NCCN	13.37	674.7
HCN	13.60	712.9
F_3CCN	13.93	688.4

[a] From ref 26.

BF_3 has a B−N distance of 2.01 Å and an N−B−F angle of 95.6° in the gas phase,[3] and these values clearly lie between those for fairly strong complexes such as $H_3N{-}BF_3$[24] and "van der Waals complexes" such as $N_2{-}BF_3$.[25] Yet another remarkable feature of these complexes is that they undergo dramatic structural changes upon crystallization. For HCN−BF_3, the gas-phase B−N distance is 2.47 Å,[14] but it contracts to 1.65 Å upon crystallization.[15]

Such large gas−solid structural differences raise the question as to how a solvent or other bulk, condensed-phase medium may affect these systems, and our work has been concerned mainly with the effects of inert cryogenic matrices.[11,23] For $CH_3CN{-}BF_3$ in solid argon,[11] a comparison of the matrix-IR frequencies with those measured for the solid and those calculated for the two minimum-energy gas-phase structures (at the B3LYP/aug-cc-pvqz level)[12] indicate that the matrix does indeed induce a considerable contraction of the B−N bond. At this point, we turn to singly halogenated derivatives of $CH_3CN{-}BF_3$, i.e., $X{-}CH_2CN{-}BF_3$, where X = F, Cl, Br, and I. From a simple induction standpoint, one would expect these species to be weaker electron donors than CH_3CN, in contrast to nitriles with larger organic substituents, (e.g., $(CH_3)_3CCN$ and C_6H_5CN). We have recently found that $(CH_3)_3CCN{-}BF_3$ and $C_6H_5CN{-}BF_3$ have dative bonds that are somewhat stronger than that in $CH_3CN{-}BF_3$, and as a result, the condensed-phase effects on their structural properties are somewhat less pronounced.[23]

Beyond simple inductive effects, the ionization energies and proton affinities[26] listed in Table 1 for select nitriles and NH_3 (as a strong-base reference point) impart a conflicting picture of relative Lewis base strength among $X{-}CH_2CN$ species. For example, the ionization energy of CH_3CN lies between those of FCH_2CN and $ClCH_2CN$, but the proton affinity of $ClCH_2CN$ is actually much lower than that of CH_3CN. This effect stems from an increasing amount of halogen p-orbital character of the highest occupied molecular orbitals (HOMOs) as one proceeds from F− to $BrCH_2CN$ (Figure 1). In turn, the ionization potentials decrease because the halogen p orbitals are higher in energy (i.e., they have less-negative energy values). However, the nitrile moiety still bears a large partial negative partial charge, irrespective of halogen substitution, and is thus the most likely bonding site for hard Lewis acids. Nonetheless, the HOMOs do suggest that the XCH_2CN species are potentially bifunctional donors and may coordinate to soft Lewis acids via the halogen. Ultimately, it is clear that these compounds should show rich coordination behavior.

Figure 1. HOMOs for F−, Cl−, and Br−CH_2CN (HF/6-311G*).

While our long-term goal is to assess the effects of inert, condensed-phase environments on the structural properties of $XCH_2CN{-}BF_3$ complexes, at this point, we lack benchmark gas-phase or solid-state data for these systems to compare with our forthcoming matrix isolation−IR results. Here we present gas-phase structures and frequencies obtained from density functional calculations, solid-state structures from single-crystal X-ray crystallography, and solid-state IR spectra for several of these complexes. These results suggest, even in the absence of experimental, gas-phase data, that very large structural changes do indeed occur in these systems upon crystallization and that large vibrational frequency shifts parallel these changes.

II. Experimental Section

Materials. FCH_2CN (98%), $ClCH_2CN$ (99%), $BrCH_2CN$ (97%), and ICH_2CN (98%) were obtained from Aldrich and were subjected to a few freeze−pump−thaw cycles prior to use. BF_3 (99.5+%) was also obtained from Aldrich, and N_2 (standard purity) was obtained from Praxair. Both gases were used without any additional purification.

Preparation and Handling of Crystalline Samples. Solids were prepared by first adding about 3−5 mL of liquid nitrile to a 50 or 100 mL Schlenk tube. The top of the tube was fitted with a rubber septum. Gases were introduced through the septum via a small hypodermic needle and were allowed to vent through a sidearm (and into a fume hood) by slightly opening a Teflon stopcock. Initially, the tube was purged with a steady flow of N_2 for several minutes to displace ambient air. Then, BF_3 was slowly introduced to the tube in a similar manner. In the case of the Br- and I-containing derivatives, solids formed immediately at the bottom of the tube, but for the F and Cl complexes, no obvious signs of reaction were apparent aside from a slight warming. In any event, the BF_3 flow was continued for a few additional minutes to ensure a slight excess, and it was clear (via white fumes from the sidearm) that most of the nitrogen had been displaced. The excess BF_3 was allowed to remain in the tube, and the sample tube was sealed and stored at reduced temperature for several days to allow for crystal growth. For the I, Br, and Cl species, optimum crystal growth occurred when the tubes were kept in a cold room at 4−5 °C. For $FCH_2CN{-}BF_3$, slightly colder temperatures were found to be optimal, approximately 0 °C. All the compounds were found to be unstable and rather difficult to handle, especially $FCH_2CN{-}BF_3$ and $ClCH_2CN{-}BF_3$, as they were apt to decompose upon warming and seemed to react with ambient water vapor. As a result, each required special handling at low temperature to obtain and preserve

(24) Fujiang, D.; Fowler, P. W.; Legon, A. C. *J. Chem. Soc., Chem. Commun.* **1995**, 113.
(25) Janda, K. C.; Bernstien, L. S.; Steed, J. M.; Novick, S. E.; Klemperer, W. *J. Am. Chem. Soc.* **1978**, *100*, 8074.
(26) The NIST Chemistry Webbook. http://webbook.nist.gov/chemistry (accessed December 2004).

Table 2. X-Ray Crystallographic Data for Haloacetonitrile−BF_3 Complexes[a]

complex	FCH_2CN-BF_3	$ClCH_2CN-BF_3$	ICH_2CN-BF_3
empirical formula	$C_2H_2BF_4N$	$C_2H_2BClF_3N$	$C_2H_2BF_3IN$
fw	126.86	143.31	234.76
cryst syst	monoclinic	triclinic	monoclinic
space group	$P2_1$	$P\bar{1}$	$P2_1/c$
a (Å)	5.173(1)	7.499(1)	9.947(2)
b (Å)	5.754(1)	7.682(1)	8.240(1)
c (Å)	7.927(2)	9.275(1)	7.671(4)
α (deg)		106.66(1)	
β (deg)	99.00(2)	90.39(1)	108.96(2)
γ (deg)		90.39(1)	
V (Å^3)	233.05(8)	519.2(2)	594.6(3)
Z	2	4	4
T (K)	173(2)	173(2)	173(2)
calcd density (g·cm^{-3})	1.808	1.833	2.622
cryst size (mm)	0.40 × 0.35 × 0.10	0.62 × 0.30 × 0.05	0.20 × 0.20 × 0.04
absorption coefficient (mm^{-1})	0.220	0.680	5.338
2θ max (deg)	50.02	49.86	49.42
No. of reflns collected	899	1953	983
No. of independent reflns	806	1804	950
No. of reflns with $I > 2\sigma(I)$	681	1615	742
No. of variables	73	146	73
R1 (wR2) [$I > 2\sigma(I)$] [b]	0.0517 (0.1293)	0.0328 (0.0855)	0.0437 (0.1017)
R1 (wR2) [all data]	0.0643 (0.1382)	0.0385 (0.0897)	0.0676 (0.1104)
GOF	1.078	1.088	1.055
difference peaks (e$^-$·Å^{-3})	0.194, −0.216	0.448, −0.431	0.890, −0.887

[a] See Experimental Section for additional data collection, reduction, structure solution, and refinement details. [b] $R1 = \sum||F_o| - |F_c||/\sum|F_o|$; $wR2 = [\sum[w(F_o^2-F_c^2)^2]]^{1/2}$ where $w = 1/\sigma^2(F_o^2) + (aP)^2 + bP$.

appropriate samples for crystallographic characterization. A single crystal of FCH_2CN-BF_3 was selected by immersing a vial containing the solid in liquid nitrogen, transferring multiple potential samples to the tip of a precooled spatula, and selecting an appropriate single crystal while blanketing the spatula with a stream of cold nitrogen gas. A single crystal of $ClCH_2CN-BF_3$ was selected by examining the bulk sample using a locally designed cold stage, cooled to a temperature below −70 °C with cold nitrogen gas. Samples of ICH_2CN-BF_3 were somewhat less thermally sensitive. A crystal of this complex was selected by examining the bulk sample while covered by a generous film of chilled (0 °C) heavyweight oil to protect the crystalline material from the atmosphere. Crystalline samples of $BrCH_2CN-BF_3$ could also be prepared and examined in anticipation of a crystallographic structure determination, and several data sets were collected for this complex, but an as-yet-unresolved twinning issue prevented successful determination of the structure.

Crystallographic Data Collection, Structure Solution, and Refinement. Crystals of each of the three complexes, selected as described above, were mounted on the end of a thin-walled glass capillary and transferred to a Bruker-Nonius MACH3S diffractometer equipped with graphite-monochromated Mo Kα radiation (λ = 0.71073 Å) for data collections at −100 °C. Unit cell constants were determined from a least squares refinement of the setting angles of 25 high-angle, machine-centered reflections. Intensity data were collected using the $\omega/2\theta$ scan technique to a maximum 2θ value of ∼50°. Corrections for crystal decay were not required. For $ClCH_2CN-BF_3$ and ICH_2CN-BF_3, absorption corrections based on azimuthal scans of several reflections were applied, resulting in transmission factors between 1.0 and 0.8007 ($ClCH_2CN-BF_3$) or 1.0 and 0.6896 (ICH_2CN-BF_3). The intensity data were corrected for Lorentz and polarization effects and converted to structure factors using the CrystalStructure suite of programs.[27]

Space groups for each complex were determined on the basis of systematic absences and intensity statistics. Successful direct methods solutions were calculated, which provided the positions of most non-hydrogen atoms directly from the E-map. Remaining atoms were located following several cycles of least squares refinement and structure expansion using the SHELXTL suite of programs.[28] Hydrogen atoms were added geometrically. All non-hydrogen atoms were refined with anisotropic displacement parameters. Carbon-bound hydrogen atoms were refined as riding atoms with group isotropic displacement parameters fixed at 1.2 × U(eq) of the host carbon atom. The asymmetric units of FCH_2CN-BF_3 and ICH_2CN-BF_3 contain a single formula unit of each of the complex, while two crystallographically independent complexes are found in the asymmetric unit of $ClCH_2CN-BF_3$. In the final stages of refinement of ICH_2CN-BF_3, a number of low-angle $hk0$ reflections were excluded from the refinement as the F_o's of these reflections were systematically larger than their F_c's. This behavior was ascribed to the presence of a small satellite crystal that could not be mechanically separated from the larger specimen. Relevant structure determination information for the complexes is presented in Table 2. Selected interatomic distances and angles and thermal ellipsoid representations of the refined structures are shown below. Full details of the structure determinations, in CIF format, are provided as Supporting Information.

Solid-State IR Spectra. Infrared spectra were collected using a previously described matrix isolation−IR apparatus,[11,23] which consists of a Cryomech ST15 optical cryostat fitted with KBr windows (both internal and external). Temperature was measured and controlled using a Scientific Instruments 9600-1 temperature controller and a single Si diode located at the end of the second refrigeration stage. Spectra were collected with a Nicolet Avatar 360 FTIR, at 1.0 cm^{-1} resolution, and typically, 100 scans were averaged for both sample and background data. The observed peak maxima were reproducible to ±4 cm^{-1}. The cryostat apparatus is assembled on a movable cart, which is wheeled into the spectrometer sample compartment for each spectrum. As such, interference from ambient water vapor and CO_2 in the unpurged beam path can be problematic in the case of weak absorbance signals.

(27) *CrystalStructure*, version 3.6.0; Rigaku Corporation and Rigaku/MSC: The Woodlands TX, 2004.

(28) *SHELXTL*, version 6.10; Bruker AXS: Madison, WI, 2000.

Thin films of the bulk solids were prepared by first making a dilute gas mixture containing nitrile, BF_3, and argon on a vacuum line. For the Cl- and F-containing species, mixtures containing approximately 0.5% nitrile, 0.5% BF_3, and 99% argon, were used, though in some cases, a slight excess of nitrile was added to minimize peaks due to unreacted BF_3 (between 1450 and 1500 cm^{-1}). For $BrCH_2CN-BF_3$, the mixtures were more dilute, typically 0.2% $BrCH_2CN$ and BF_3, since the vapor pressure of $BrCH_2CN$ is much lower that of FCH_2CN and $ClCH_2CN$. Films were deposited directly onto the cold (120 K) KBr sample window by flowing the gas mixtures into the cryostat vaccum chamber at a rate of roughly 5 mmol/h. Argon does not condense on the sample window at this temperature; thus, only the nitrle and BF_3 are deposited. Like $(CH_3)_3CCN-BF_3$ and $C_6H_5CN-BF_3$,[23] the spectra obtained closely resemble low-temperature, solid-state IR spectra of CH_3CN-BF_3,[6] indicating that the majority of the sample consists of nitrile−BF_3 complexes, though the very bright vibrational bands of excess, unreacted BF_3 were also observed in some experiments.

III. Computational Methods

The HF/6-311G* orbitals displayed in Figure 1, as well as preliminary B3LYP[29] calculations on the $X-CH_2CN-BF_3$ (X = F, Cl, Br) systems using Pople basis sets (6-31G*, 6-31+G*, 6-311G*, and 6-311+G**)[29,30] were performed using SPARTAN '02 (Macintosh v 1.0.3, and Windows v 1.0.1).[31] Aside from this preliminary work, all other computations were performed using Gaussian03,[32] which enabled the use of several additional density functional methods, larger basis sets, and tighter convergence criteria for geometry optimizations. Version b.0.1 was used for MP2 and all density functional methods except O3LYP,[29] for which version c.0.3 was used. An ultrafine grid was employed for all DFT calculations in Gaussian, and convergence criteria for optimizations (except as noted) were set using the "opt=tight" option (which sets the maximum and RMS forces to 1.5×10^{-5} and 1.0×10^{-5} hartrees/bohr, respectively, and the maximum and RMS displacements to 6.0×10^{-5}, and 4.0×10^{-5} bohr, respectively). The aug-cc-pVTZ basis set[29,33] was used for most Gaussian03 calculations, although the cc-pVTZ basis set[33] was also used for DFT calculations on FCH_2CN-BF_3 to examine the effect of diffuse functions (signified by "aug-") on the structural results. The analogous double-ζ basis sets (cc-pVDZ, and aug-cc-pVDZ)[33] were also used for some MP2 calculations on FCH_2CN-BF_3, including those in which we explored the relative stability of F-bonded isomeric structures.

IV. Results and Discussion

Computational Structure Results. Initial B3LYP calculations indicated that all complexes were slightly bent about the C−N−B linkage and, moreover, that the torsional degree of freedom was extremely flat. Thus, to be systematic in our search for the minimum-energy structures, we conducted four parallel sets of optimizations, each starting with the C−N−B angles set to 180° in either the eclipsed or staggered conformation, and with or without enforcing C_s symmetry. The staggered forms were found to be most stable at the B3LYP/6-311+G** level, but by only a few calories per mole (0.005 kcal/mol in the case of FCH_2CN-BF_3). Furthermore, each complex was indeed bent slightly along the C−N−B linkage by about 2°, so the conformers are not strictly "eclipsed" or "staggered" in the formal sense. Nonetheless, we retain these terms throughout for the sake of simplicity.

At this point, we identified two reasons to be concerned with these B3LYP results. First of all, B3LYP results for CH_3CN-BF_3 lacked complete convergence with even larger basis sets, up to aug-cc-pVQZ.[12] Furthermore, a recent study of amine−borane systems cast doubt on the performance of B3LYP for B−N dative bonds.[34] Thus, we conducted a survey of various DFT methods (and MP2 with somewhat smaller basis sets) on the equilibrium structure of staggered FCH_2CN-BF_3 (C_s) under the presumption that some degree of consistency would emerge. Table 3 lists equilibrium B−N distances obtained in this survey, and overall, there is a considerable degree of inconsistency among the various methods. For the most part, however, B−N distances are a few hundredths of an angstrom shorter when diffuse functions are used (i.e., aug-cc-pVTZ), and this has been noted in several previous instances for nitrile−BF_3 systems.[12,21−23] Regardless, in the absence of an experimental structure, it was unclear which method was most reliable. To address this ambiguity, we conducted (and recently completed) a validation study on $HCN-BF_3$,[22] a similar and also fairly weak complex for which an experimental structure has been determined.[14] In that work, we found that several hybrid DFT/HF methods (B3LYP, B3PW91, B98, and *m*PW1PW91)[29] yielded structures that agreed favorably with experiment, with B3PW91 providing the best agreement, even superior to MP2 (with the aug-cc-pVTZ basis set).

For the most part, the results in Table 3 track those obtained for $HCN-BF_3$,[22] and thus, we chose to utilize B3PW91/aug-cc-pVTZ as our preferred method for this study. For completeness sake, we obtained B3LYP/aug-cc-pVTZ and *m*PW1PW91/aug-cc-pVTZ results as well. Selected structure parameters of both the eclipsed and staggered conformers from all three methods are listed in Table 4, and complete, minimum-energy B3PW91/aug-cc-pVTZ structures are displayed in Figure 2. For the F- and Cl-containing

(29) For a recent overview of density functional theory and other computational methods and basis sets used in this work, see: Cramer, C. J. *Essentials of Computational Chemistry*, 2nd ed.; John Wiley and Sons: Sussex, 2004, and references therein.

(30) (a) Krishnan, R.; Binkley, J. S.; Seeger, R.; Pople, J. A. *J. Chem. Phys.* **1980**, *72*, 650.

(31) *SPARTAN '02*; Wavefunction, Inc.: Irvine, CA, 2002.

(32) Frisch, M. J.; Trucks, G. W.; Schlegel, H. B.; Scuseria, G. E.; Robb, M. A.; Cheeseman, J. R.; Montgomery, J. A., Jr.; Vreven, T.; Kudin, K. N.; Burant, J. C.; Millam, J. M.; Iyengar, S. S.; Tomasi, J.; Barone, V.; Mennucci, B.; Cossi, M.; Scalmani, G.; Rega, N.; Petersson, G. A.; Nakatsuji, H.; Hada, M.; Ehara, M.; Toyota, K.; Fukuda, R.; Hasegawa, J.; Ishida, M.; Nakajima, T.; Honda, Y.; Kitao, O.; Nakai, H.; Klene, M.; Li, X.; Knox, J. E.; Hratchian, H. P.; Cross, J. B.; Bakken, V.; Adamo, C.; Jaramillo, J.; Gomperts, R.; Stratmann, R. E.; Yazyev, O.; Austin, A. J.; Cammi, R.; Pomelli, C.; Ochterski, J. W.; Ayala, P. Y.; Morokuma, K.; Voth, G. A.; Salvador, P.; Dannenberg, J. J.; Zakrzewski, V. G.; Dapprich, S.; Daniels, A. D.; Strain, M. C.; Farkas, O.; Malick, D. K.; Rabuck, A. D.; Raghavachari, K.; Foresman, J. B.; Ortiz, J. V.; Cui, Q.; Baboul, A. G.; Clifford, S.; Cioslowski, J.; Stefanov, B. B.; Liu, G.; Liashenko, A.; Piskorz, P.; Komaromi, I.; Martin, R. L.; Fox, D. J.; Keith, T.; Al-Laham, M. A.; Peng, C. Y.; Nanayakkara, A.; Challacombe, M.; Gill, P. M. W.; Johnson, B.; Chen, W.; Wong, M. W.; Gonzalez, C.; Pople, J. A. *Gaussian 03*, revision B.03; Gaussian, Inc.: Wallingford, CT, 2004.

(33) Woon, D. E.; Dunning, T. H., Jr. *J. Chem. Phys.* **1993**, *98*, 1358.

(34) Gilbert, T. M. *J. Phys. Chem. A.* **2004**, *108*, 2550.

Table 3. Equilibrium B−N Distances of FCH_2CN-BF_3 Obtained Using Various Computational Methods[a]

method	basis set	R(B−N) (Å)
MP2	cc-pVDZ	2.431
	aug-cc-pVDZ	2.318
	cc-pVTZ	2.387
	Hybrid DFT Methods	
B3LYP	cc-pVTZ	2.525
	aug-cc-pVTZ	2.514
B3PW91	cc-pVTZ	2.445
	aug-cc-pVTZ	2.423
MPW1K	cc-pVTZ	2.283
	aug-cc-pVTZ	2.250
*m*PW1PW91	cc-pVTZ	2.365
	aug-cc-pVTZ	2.338
O3LYP	cc-pVTZ	2.926
	aug-cc-pVTZ	2.975
	Pure DFT Methods	
*m*PWPW91	cc-pVTZ	2.452
	aug-cc-pVTZ	2.421
BPW91	cc-pVTZ	2.548
	aug-cc-pVTZ	2.524
BLYP	cc-pVTZ	2.630
	aug-cc-pVTZ	2.623
OLYP	cc-pVTZ	3.106
	aug-cc-pVTZ	3.189

[a] These results are for the nearly staggered conformer (C_s symmetry), which was ultimately found to be slightly higher in energy than the nearly eclipsed form. For B3PW91 (see below), the B−N distance differs by less than 0.001 Å between the two conformers. See text for discussion.

species, the B3LYP, B3PW91, and *m*PW1PW91 results exactly parallel the $HCN-BF_3$ results. Specifically, the B3LYP results for the B−N distance are about 0.1 Å longer and those from *m*PWPW91 and about 0.1 Å shorter. In the case of $BrCH_2CN-BF_3$, the *m*PW1PW91/aug-cc-pVTZ bond length is much shorter, 1.88 Å, but interestingly, the *m*PW1PW91/cc-pvtz bond length is 2.34 Å (for either conformer). This extreme sensitivity to diffuse functions, well beyond that noted above, is reminiscent of CH_3CN-BF_3,[12] in which the effect stems from a very flat B−N distance potential. Though it only occurs for one of three functionals for $BrCH_2CN-BF_3$, it may indicate that the B−N distance potential is rather flat and worthy of a more detailed examination in the future. For now, we conclude that the minimum energy structure has a B−N distance near 2.34 Å.

For each complex, the eclipsed form seems to be the lowest in energy, in contrast to our initial assessment based on B3LYP/6-311+G**, but the energy difference is still only a few calories per mole and arguably beyond the accuracy of the computations. It is worth noting that torsional frequencies obtained for the eclipsed forms (see below) are all real, but in the case of $ClCH_2CN-BF_3$, the staggered frequencies were found to be real as well. Effectively, these complexes are best viewed as free rotors. Moreover, the torsional conformation has very little impact on the structural parameters with which we are mainly concerned (i.e., the B−N distance and N−B−F angle).

We also attempted to locate a minimum-energy structure of FCH_2CN-BF_3 in which the BF_3 was bonded to the F (i.e., $NCCH_2F-BF_3$). Using MP2, with double-ζ basis sets, a symmetric (C_s) structure was found that had an intermolecular B−F distance of about 2.4 Å. The F atoms of the BF_3 group were directed toward the H's on FCH_2CN, suggestive of a very weak H-bonding interaction, at a distance of about 2.75 Å. This structure was found to be 1.8 kcal/mol higher in energy than the N-bonded form (at the MP2/aug-cc-pVDZ level). We also calculated the energy difference between these structures at the MP2/aug-cc-pVTZ level and found that the F-bonded structure was 2.6 kcal/mol higher in energy. While DFT methods may be suspect given this apparently weak F−B interaction, we note that the energy difference between the analogous structures was also 2.6 kcal/mol at the B3PW91/aug-cc-pVTZ level. (The F-bonded structure was obtained using default convergence criteria.) Given the energy differences and the observation that all of the crystalline complexes are N-bonded (below), we did not examine the Cl and Br derivatives for analogous structures.

For all of the gas-phase complexes, the B−N distances are long and the N−B−F angles are just slightly larger than 90°, indicating that these complexes are fairly weakly bonded in the gas phase. However, we neglected to calculate absolute binding energies since neither DFT nor MP2 were found to be accurate for $HCN-BF_3$ compared to very highly correlated levels of electronic structure theory.[22] Nevertheless, there are slight yet very clear trends that suggest that the dative bonds do become stronger in proceeding from FCH_2CN-BF_3 to $BrCH_2CN-BF_3$, as would be expected on the basis of simple inductive arguments. For example, the (B3PW91/aug-cc-pVTZ) B−N distance is predicted to be 2.422 Å in FCH_3CN-BF_3, 2.374 Å in $ClCH_2CN-BF_3$, and 2.341 Å in $BrCH_2CN-BF_3$, and in turn, the N−B−F angles open by a few tenths of a degree (on average) across the three complexes. The B−F distances are only a few thousandths of an angstrom longer than that calculated for free BF_3 at the B3PW91/aug-cc-pvVTZ level of theory,[22] but they do increase very slightly across the series. Interestingly, the degree of bend about the C−N−B linkage is essentially identical among the three complexes.

As a whole, these complexes appear to be just a bit more strongly bonded than $HCN-BF_3$, yet much weaker than CH_3CN-BF_3. This trend is at odds with the ionization potential data (Table 1) but is consistent with proton affinity data (though such data are only available for CH_3CN and $ClCH_2CN$). This can be rationalized by recalling the char-

Table 4. Selected Structural Parameters and Relative Conformational Energies for F−, Cl−, and Br−CH_2CN−BF_3 from B3LYP, B3PW91, and *m*PW1PW91 Calculations

method[a]	conformer [b]	*E* (cal/mol)[c]	*R*(B−N) (Å)	<NBF′ (°) [d]	<NBF″ (deg) [d]	<CNB (deg)
			FCH_2CN−BF_3			
B3LYP	eclipsed	0.0	2.513	93.4	93.0	178.2
	staggered	0.7	2.514	92.6	93.4	178.0
B3PW91	**eclipsed**	**0.0**	**2.422**	**94.1**	**93.7**	**178.2**
	staggered	1.4	2.423	93.4	94.1	178.1
*m*PW1PW91	eclipsed	0.0	2.337	94.7	94.3	178.2
	staggered	2.0	2.338	94.0	94.7	178.0
			$ClCH_2CN$−BF_3			
B3LYP	eclipsed	0.0	2.487	93.6	93.2	178.2
	staggered	2.9	2.488	93.0	93.5	178.3
B3PW91	**eclipsed**	**0.0**	**2.374**	**94.6**	**94.1**	**178.2**
	staggered	3.7	2.375	93.9	94.4	178.2
*m*PW1PW91	eclipsed	0.0	2.260	95.5	93.2	178.2
	staggered	4.6	2.262	94.9	95.4	178.2
			$BrCH_2CN$−BF_3			
B3LYP	eclipsed	0.0	2.473	93.8	93.3	178.2
	staggered	2.6	2.473	93.1	93.6	178.4
B3PW91	**eclipsed**	**0.0**	**2.341**	**94.8**	**94.5**	**178.3**
	staggered	46.6	2.343	94.3	94.7	178.3
*m*PW1PW91	eclipsed	0.0	*1.879*	*100.4*	*100.1*	178.6
	staggered	194.4	*1.881*	*99.9*	*100.3*	174.2

[a] The aug-cc-pVTZ basis set was used for these results. [b] Approximate conformation. See text for discussion. [c] Energy relative to the lower-energy conformer. [d] <NBF′ is the N−B−F angle in the plane of symmetry, <NBF″ is the out-of-plane N−B−F angle.

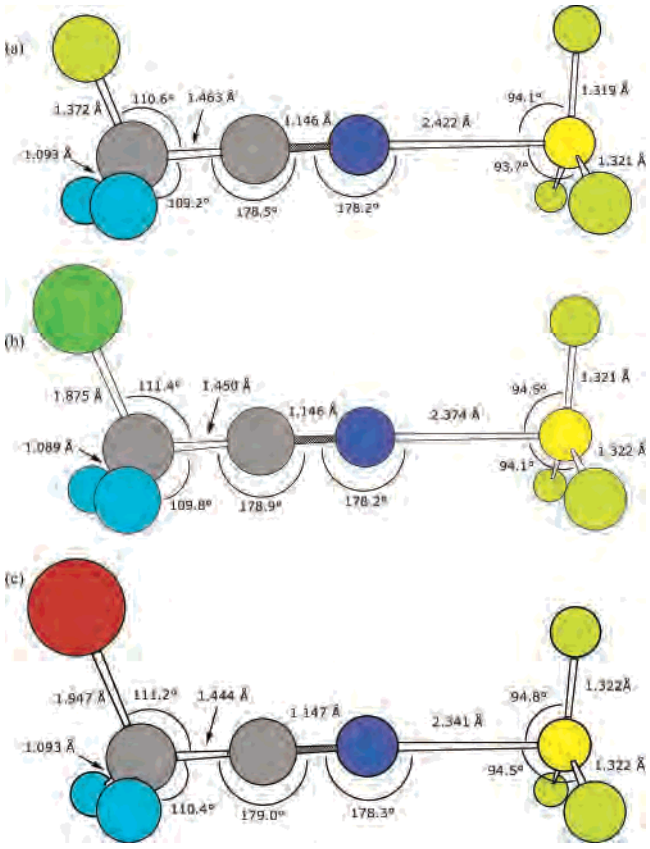

Figure 2. Gas-phase (B3PW91/aug-cc-pVTZ) structures of FCH_2CN−BF_3 (a), $ClCH_2CN$−BF_3 (b), and $BrCH_2CN$−BF_3 (c).

acteristics of the HOMOs, as discussed above and depicted in Figure 1. That is, ionization potentials decrease from F−CH_2CN to Br−CH_2CN but do so because the HOMOs have more halogen character and less amplitude on the nitrile moiety. As far as electrostatics are concerned, however, it appears that the nitrogen bears more negative charge than the halogens, even in FCH_2CN, though the difference is very slight. At the B3PW91/aug-cc-pVTZ level, the Mulliken charge on the N in FCH_2CN is −0.38, while that on the F is −0.37. In proceeding to $BrCH_2CN$, the amount of negative charge on the N increases only slightly, to −0.41, while the charge on the Br increases to +0.03. Considering that BF_3 and H^+ are both hard acids,[35] it is reasonable that the structural trends follow proton affinity data since BF_3 prefers coordination with the nitrogen, which appears to be more favorable in terms of electrostatics. It is worth noting in this context that Leopold and co-workers have argued (using data for SO_3 complexes) that it is key to examine the ionization potential of the actual donor orbital (not necessarily the HOMO) in attempts to correlate structural properties with orbital energy gaps.[36] However, we were unable to locate any ionization potential data that would provide energies for the lower-lying σ-CN-type orbitals. Moreover, like the π-CN-type HOMOs, mixing between σ_{CN} and the halogen p orbitals (especially F in this case) complicates any analysis of the DFT orbital energies.

Solid-State Structures. The solid-state structures of FCH_2CN−BF_3, $ClCH_2CN$−BF_3, and ICH_2CN−BF_3 were determined by X-ray crystallography. In addition to confirming the atomic connectivity in these complexes, these structure determinations allow us to probe potential structural changes that occur upon deposition and characterize structural trends that are concomitant with changes in the carbon-bound halogen atom. The crystallographic results are summarized in Table 2, while significant interatomic distances and angles are presented in Table 5. Full details of the structure determinations, in CIF format, are provided as Supporting Information.

Thermal ellipsoid representations of the three X-ray crystal structures are presented in Figure 3. In each case, the

(35) Pearson, R. G., Ed. *Hard and Soft Acids and Bases*; Dowden, Hutchinson and Ross, Inc.: Stroudsburg, PA, 1973.
(36) Hunt, S. W.; Leopold, K. R. *J. Phys. Chem. A* **2001**, *105*, 5498.

Table 5. Significant Interatomic Distances (Å) and Angles (deg) for Haloacetonitrile−BF_3 Complexes[a]

complex	FCH_2CN-BF_3	$ClCH_2CN-BF_3$ (a)	$ClCH_2CN-BF_3$ (b)	ICH_2CN-BF_3
B−F(1)	1.340(6)	1.358(3)	1.345(3)	1.374(12)
B−F(2)	1.362(6)	1.355(3)	1.355(3)	1.341(13)
B−F(3)	1.354(6)	1.364(3)	1.354(3)	1.356(13)
B−N	1.635(6)	1.649(2)	1.640(3)	1.643(12)
N−C(1)	1.130(5)	1.132(3)	1.137(3)	1.124(11)
F(1)−B−F(2)	113.2(4)	113.6(2)	114.7(2)	114.0(8)
F(1)−B−F(3)	113.5(4)	112.3(2)	112.5(2)	112.4(9)
F(2)−B−F(3)	112.3(4)	113.7(2)	111.7(2)	114.5(9)
F(1)−B−N	105.7(4)	105.9(2)	105.7(2)	103.3(8)
F(2)−B−N	105.0(3)	105.1(2)	105.8(2)	105.3(8)
F(3)−B−N	106.2(3)	105.3(2)	105.5(2)	106.1(7)
B−N−C(1)	179.7(4)	175.2(2)	176.3(2)	174.2(9)

[a] Metrical details for each of the crystallographically independent molecules of $ClCH_2CN-BF_3$ are provided separately as molecule (a) and molecule (b).

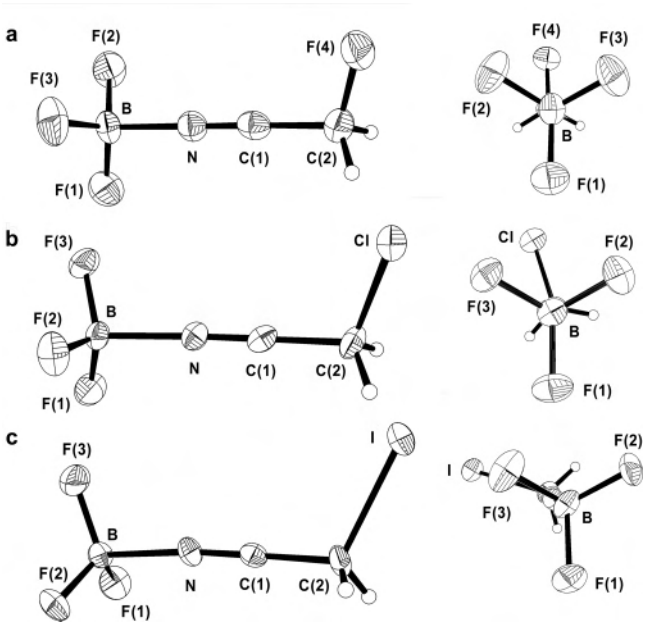

Figure 3. Views of the X-ray crystal structures of the haloacetonitrile−BF_3 complexes drawn at the 50% probability levels for all non-hydrogen atoms.

haloacetonitrile−BF_3 complexes are found with the Lewis acidic BF_3 unit bound to the nitrile nitrogen, even though each haloacetonitrile features two potentially Lewis basic sites. In general, the metrical parameters for the complexes very closely resemble those previously determined for CH_3CN-BF_3(s),[4] HCN−BF_3(s),[15] and $C_6H_5CN-BF_3$(s),[23] with B−N distances near 1.65 Å and N−B−F angles between 105° and 106°. Thus, introduction of the halogen substituent does not cause dramatic changes in the solid-state structural properties of the complexes relative to those of previously examined nitrile−BF_3 complexes.

Comparison of the calculated gas-phase and crystallographically determined solid-state structures of FCH_2CN-BF_3 and $ClCH_2CN-BF_3$ reveals that major structural changes occur upon deposition of the complexes from the vapor phase. For FCH_2CN-BF_3 (Figure 3a) the solid-state B−N distance is 1.635(6) Å, which is 0.78 Å shorter than in the calculated gas-phase structure. Furthermore, the N−B−F angles are 11.7° larger (on average) in the solid. These gas−solid structural differences rival those of HCN−BF_3,[14,15] the most extreme case in this class of compounds. Besides the B−N distance and N−B−F angles, there are also some subtle structural changes that occur within the nitrile and BF_3 subunits that are associated with shortening and strengthening of the B−N bond. Specifically, the C−N distance contracts by about 0.01 Å, an effect noted previously in CH_3CN-BF_3,[3] and the B−F bonds lengthen by about 0.03 Å (both relative to the B3PW91/aug-cc-pVTZ structure). The C−N−B linkage straightens upon crystallization, yielding a B−N−C bond angle of 179.7(4)°. Furthermore, the staggered conformer is observed exclusively in the solid-state (the F4−C2···B1−F3 torsion angle is 62.5°), and we observe no evidence of any thermal averaging in the crystal used for the structure determination.

Comparable gas−solid structural differences are also apparent for $ClCH_2CN-BF_3$ (Figure 3b). The B−N distance in this solid complex is 1.640(3) Å, which is 0.73 Å shorter than in the calculated gas-phase structure, while the N−B−F angles are 11.2° larger (on average) in the solid. As observed in FCH_2CN-BF_3, some slight structural changes occur in the nitrile and BF_3 subunits of $ClCH_2CN-BF_3$ that reflect a stronger B−N interaction in the crystalline complex. Specifically, the B−F distances increase by approximately 0.04 Å, while the C−N distance decreases by 0.01 Å. Finally, each of the two crystallographically independent formula units of $ClCH_2CN-BF_3$ is twisted away from idealized eclipsed or staggered conformations: the Cl−C2···B1−F3 torsion angle is 41.7° in one complex and 23.4° in the second independent molecule.

Inspection of the X-ray crystal structure of ICH_2CN-BF_3 (Figure 3c) reveals an extension of two structural trends that exist within this group of three haloacetonitrile−BF_3 complexes. Specifically, the complex exists in the most nearly eclipsed rotational conformation (the I−C2···B1−F3 torsion angle is 12.8°) and the B−N−C bond angle exhibits the largest deviation from linearity among the three complexes. The factors that influence the rotational conformations of the three complexes are unclear. However, it may be that observation of the three different rotomers in the X-ray crystal structures of FCH_2CN-BF_3, $ClCH_2CN-BF_3$, and ICH_2CN-BF_3 reflects the relatively flat torsional potential discussed in the computational section above. The slight bend of the B−N−C bond angle may result from intramolecular or intermolecular effects. We note that ICH_2CN-BF_3 and

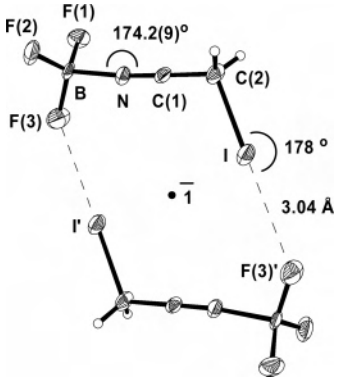

Figure 4. I···F intermolecular interactions in ICH_2CN-BF_3.

$ClCH_2CN-BF_3$, which are more eclipsed than FCH_2CN-BF_3, have B−N−C angles that are both slightly nonlinear, with the BF_3 unit tilted away from the carbon-bound halogen atom. In addition, the magnitude of the deviation of the B−N−C angle from linearity in ICH_2CN-BF_3 and $ClCH_2CN-BF_3$ does appear to correlate with the progression of the complexes toward a more eclipsed conformation. Thus, one might conclude that the BF_3 unit is bending away from the intramolecular carbon-bound halogen atoms because these relatively large atoms are impinging spatially upon a BF_3 fluorine atom (specifically, F(3)). However, the long X···F distances involved (X = Cl, 5.39 Å; X = I, 5.59 Å) render this possible explanation unlikely. A more plausible explanation is that weak intermolecular interactions cause the B−N−C unit to flex slightly in the solid state. We have previously identified weak F···H interactions in the X-ray crystal structure of $C_6H_5CN-BF_3$ as being potentially responsible for the slight bending of the B−N−C angle (177.7°) in that crystalline compound. In the case of ICH_2CN-BF_3, one intermolecular interaction that might tilt the BF_3 unit away from the C≡N vector is a weak F···I interaction between two centrosymmetrically related complexes (Figure 4). It may be that tilting of the BF_3 unit away from the neighboring complex's iodine atom enhances the electrostatic interaction between the electronegative fluorine atom and the polarizable iodine atom while maintaining a nearly linear disposition of the C−I···F unit. Analogous intermolecular BF_3···H interactions occur within centrosymmetrically related pairs of $ClCH_2CN-BF_3$ complexes in the solid state, leading to a slight bending of the C≡N−B bond (average ≈ 176° for the two crystallographically independent complexes). However, a fundamentally different set of intermolecular interactions exists in the unit cell of FCH_2CN-BF_3. The lack of a crystallographic center of symmetry in this solid complex causes the principle intermolecular BF_3···H interactions to occur within infinite chains of complexes propagating parallel to the crystallographic *b* axis. Similar BF_3···H interactions occur between FCH_2CN-BF_3 complexes related by the 2_1 axis, with these interactions occurring parallel to the crystallographic *c* axis. However, none of these intermolecular interactions occur within a closely associated, centrosymmetric pair of FCH_2CN-BF_3 complexes, which perhaps underlies the linearity of this complex's C≡N−B bond angle.

Table 6. Calculated Gas-Phase and Observed Solid-State Frequencies for the BF_3-Localized Vibrations and the C−N Stretching Mode in F−, Cl−, and Br−CH_2CN-BF_3

description	frequencies (cm^{-1}) gas phase[a]	solid	shift (solid−gas)
FCH_2CN-BF_3			
BF_3 symmetric deformation (δ^s_{BF})	608	655	+47
BF_3 symmetric stretch (ν^s_{BF})	871	854	−17
BF_3 asymmetric stretch (ν^a_{BF})	1429[b]	1186	−243
C−N stretch (ν_{CN})	*2395*[c]	2375	*−20*[c]
$ClCH_2CN-BF_3$			
BF_3 symmetric deformation (δ^s_{BF})	596	653	+57
BF_3 symmetric stretch (ν^s_{BF})	869	863	−6
BF_3 asymmetric stretch (ν^a_{BF})	1423[b]	1200	−223
C−N stretch (ν_{CN})	*2395*[c]	2373	*−22*[c]
$BrCH_2CN-BF_3$			
BF_3 symmetric deformation (δ^s_{BF})	591	649	+58
BF_3 symmetric stretch (ν^s_{BF})	867	862	−5
BF_3 asymmetric stretch (ν^a_{BF})	1419[b]	1189	−230
C−N stretch (ν_{CN})	*2391*[c]	2360	*−31*[c]

[a] Calculated using the B3PW91/aug-cc-pVTZ method. [b] The higher frequency of two (A′ and A″) forms of this vibration in C_s symmetry. The other bands are 4−5 cm^{-1} lower for all three complexes. [c] The C−N stretch would be expected to blue-sift as the B−N bond contracts.[12] However, we have shown previously[22] that the B3PW91/aug-cc-pVTZ method gives unreliable results for CN stretching frequencies, irrespective of any scaling procedure. Thus, the gas-phase C−N stretching frequencies and, in turn, the predicted gas-to-solid shifts are not considered to be reliable.

Frequencies. Complete sets of calculated gas-phase frequencies and intensities (B3PW91/aug-cc-pVTZ) for the eclipsed conformers of the ^{11}B isotopomers of FCH_2CN-BF_3, $ClCH_2CN-BF_3$, $BrCH_2CN-BF_3$, are included as Supporting Information (Tables S1−S3, respectively). For the strong, structurally sensitive modes that we observed in the solid-state IR spectra, calculated frequencies are listed in Table 6 with solid-state peak maxima and gas-to-solid shifts. We note that the B3PW91/aug-cc-pVTZ method provided excellent agreement with measured gas-phase bands of BF_3, as well as MP2/aug-cc-pVTZ frequencies for $HCN-BF_3$.[22] It is apparent that shifts in the BF_3 asymmetric stretching modes (ν_{12} and ν_{23} in each complex, or ν^a_{BF} in general), as well as the BF_3 symmetric deformation, or "umbrella" mode (ν_7, or δ^s_{BF}) further support a slight increase in interaction strength in proceeding from FCH_2CN-BF_3 to $BrCH_2CN-BF_3$. It has been noted previously[12,18b] that these modes shift consistently in accord with B−N distance (or any other structural property that parallels interaction strength). The BF_3 asymmetric stretch shifts monotonically to lower frequencies as the B−N distance contracts. The calculated (B3LYP/aug-cc-pVTZ) frequency of this mode for free BF_3 (ν_3) is 1457 cm^{-1},[22] and those of the symmetric component (A′ in C_S) for the F-, Cl-, and Br-containing complexes are, 1429, 1423, and 1419 cm^{-1}, respectively. The shift of the umbrella mode is a bit peculiar; initially, it shifts to lower frequencies as the B−N distance contracts,[18b] but at shorter distances, the trend reverses and the band shifts abruptly to higher frequencies.[12] Among these fairly weak complexes, however, there is a steady red shift in proceeding from $F-CH_2CN-BF_3$ to $Br-CH_2CN-BF_3$: the calculated frequencies are 608, 596, 591 cm^{-1}, respectively. The BF_3 symmetric stretch (ν_8/ν_9, or ν^s_{BF}) is predicted to shift very

little across this series of complexes, but the calculated intensity of this mode, which is dipole-forbidden in free BF_3, does increase in proceeding from F to Br; the result of an increase in nonplanar distortion of the BF_3 subunit. The C−N stretch (ν_{14}, or ν_{CN}), which has often been the focus of previous attempts to correlate structural properties with frequency shifts in these systems,[5,13] does not shift systematically across the series. However, a gas-to-solid red shift is predicted (Table 6), which is not physically justifiable, and must stem form an inaccurate computational prediction of ν_{CN}. We have found previously that calculated frequencies of this mode are somewhat unreliable with B3PW91/aug-cc-pVTZ (and several other methods).[22] Nonetheless, we observe no significant shift among the calculated ν_{CN} frequencies, and there may be a substituent effect among free nitriles that is obscuring or counteracting a trend that would parallel the degree of binding to BF_3.

Solid-state IR spectra of FCH_2CN-BF_3, $ClCH_2CN-BF_3$, and $BrCH_2CN-BF_3$ are displayed in Figure 5 (a−c, respectively) together with simulated gas-phase spectra based on the calculated frequencies (dashed lines). Band assignments for the most prominent bands are listed directly on the plots, while peak frequencies are listed with gas-phase data in Table 6. The solid-state spectra are all quite similar and are dominated by four prominent peaks, very much like those previously measured for CH_3CN-BF_3(s),[6] $(CH_3)_3CCN-BF_3$(s),[23] and $C_6H_5CN-BF_3$(s).[23] As such, we presume that we can assign the dominant bands by comparison to the previously recorded spectra and that peak frequencies correspond to those of the ^{11}B isotopomer, which comprises 81% of the sample. The three strongest bands in each spectrum are the BF_3 asymmetric stretch (ν^a_{BF}) near 1200 cm^{-1}, the BF_3 symmetric stretch near (ν^s_{BF}) 860 cm^{-1}, and the BF_3 umbrella mode (δ^s_{BF}) near 650 cm^{-1}. The C−N stretch (ν_{CN}) is also readily apparent and is observed near 2375 cm^{-1}. In contrast, the gas-phase spectra feature only two strong, prominent bands; the BF_3 asymmetric stretch (ν^a_{BF}) and the "umbrella" mode (δ^s_{BF}), and these are shifted significantly from their solid-state counterparts, especially in the case of the BF_3 asymmetric stretching mode (ν^a_{BF}). These gas-to-solid shifts (aside from the C−N stretch as discussed above) directly parallel the structural changes predicted for FCH_2CN-BF_3 and $ClCH_2CN-BF_3$ on the basis of an explicit examination of each modes' structural dependence CH_3CN-BF_3.[12] For the BF_3 symmetric stretching mode, the gas-to-solid shifts are predicted to be quite small, but the band intensity increases dramatically upon deposition. These peaks are barely notable in the simulated gas-phase spectra but are quite prominent in the solid-state spectra. This stems from the increase in pyramidal distortion of the BF_3 unit that accompanies the contraction of the B−N bond. Moreover, though we lack a crystal structure for $BrCH_2CN-BF_3$, the IR spectrum clearly indicates that the solid-state structure of the complex resembles those for which the crystal structures have been measured.[4,15,23] Beyond the frequencies themselves and the predicted gas−solid band shifts, the characteristic relative intensity pattern of the peaks corresponding to the three prominent BF_3-localized modes provides further evidence of this assessment. Thus, there is clear evidence that $BrCH_2CN-BF_3$ also undergoes major structural changes upon deposition, even in the absence of a precise, crystallographically determined structure.

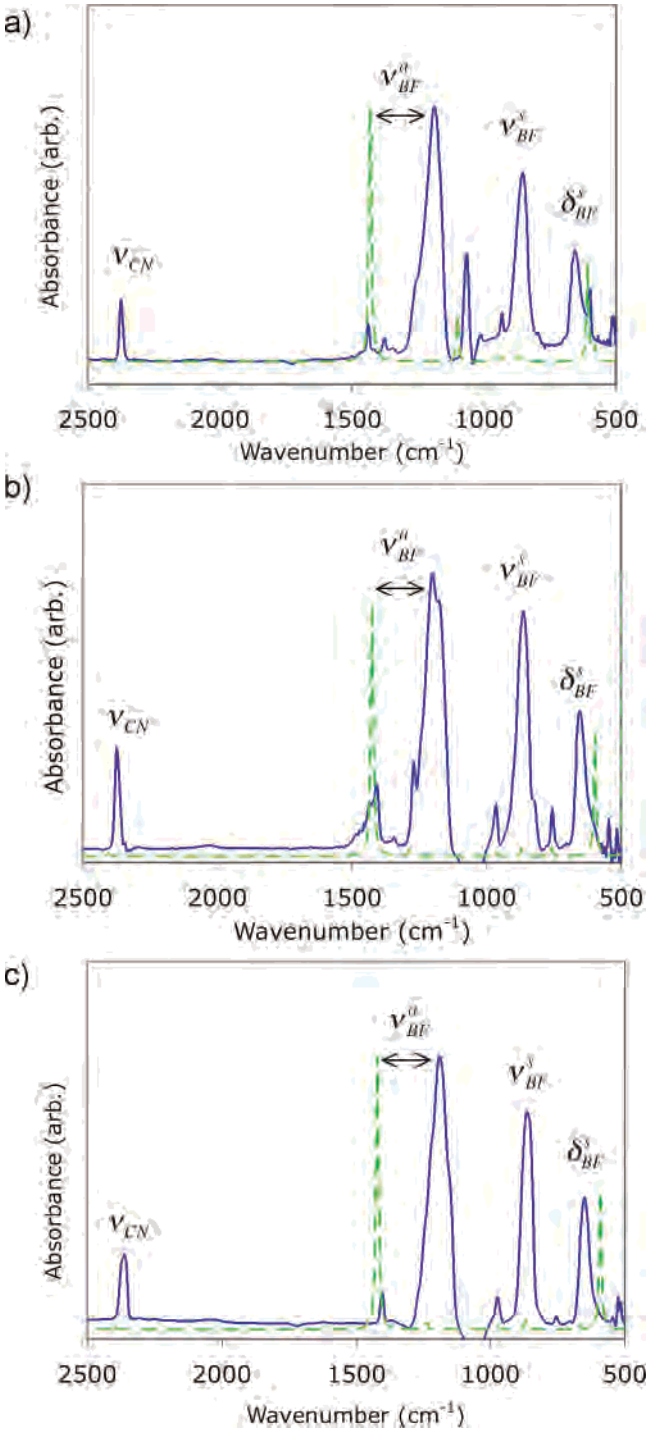

Figure 5. IR spectra of a bulk, solid samples of BF_3 and (a) FCH_2CN, (b) $ClCH_2CN$, and (c) $BrCH_2CN$, co-deposited at 120 K. The dashed spectra are simulations of the gas-phase spectra based on the calculated frequencies of the respective complexes. Peak frequencies are listed in Table 6.

V. Summary and Conclusions

We have examined the gas-phase and solid-state structural properties of the singly halogenated derivatives of CH_3CN-

BF_3 using density functional theory, crystallography, and IR spectroscopy and found that these compounds undergo major structural changes upon crystallization. Gas-phase structures from B3PW91/aug-cc-pVTZ calculations exhibit rather long B−N bond distances of 2.422, 2.374, and 2.341 Å, for $FCH_2CN−BF_3$, $ClCH_2CN−BF_3$, and $BrCH_2CN−BF_3$, respectively. These, as well as other structural properties, indicate that the complexes have fairly weak dative bonds in the gas phase but that the degree of interaction with BF_3 (as inferred from computed structural properties) does increase across the series from F− to Br−$CH_2CN−BF_3$. Collectively, these complexes are bound perhaps a bit more strongly than $HCN−BF_3$ but much more weakly than $CH_3CN−BF_3$. Both of these observations parallel proton affinity values but not ionization potential data, at least as far as HOMO orbital energies are concerned. Crystal structures very much resemble those measured previously for other nitrile−BF_3 complexes,[4,15,23] (aside from a slight bend about the C−N−B linkage), as all have short B−N bond distances of about 1.65 Å and N−B−F angles of 105−106° (on average). For $FCH_2CN−BF_3$, the B−N distance is is 1.635(6) Å, which is 0.78 Å shorter than the calculated gas-phase result. For $ClCH_2CN−BF_3$, the B−N distance is 1.640(3) Å, which is 0.73 Å shorter than the gas phase result. These changes are extreme, rivaling those observed previously for $HCN−BF_3$.[14,15] Calculated vibrational frequencies for the gas-phase complexes show subtle trends in the BF_3-localized modes that parallel the slight structural differences that occur among the F-, Cl-, and Br-containing complexes. Solid-state IR spectra show major differences in these bands for $FCH_2CN−BF_3$, $ClCH_2CN−BF_3$, and $BrCH_2CN−BF_3$. While we did not obtain a crystal structure for the Br-containing derivative, the general features of the solid-state IR spectrum, including both frequencies, as well as a characteristic intensity pattern, provide solid evidence that the complex has a similar structure to other nitrile−BF_3 complexes in the solid state and that a large gas−solid structural difference occurs for this complex as well.

Acknowledgment. We gratefully acknowledge financial support of this work from the Camille and Henry Dreyfus Foundation (Henry Dreyfus Teacher-Scholar Awards to J.A.P. and J.A.H.), the National Science Foundation (CHE-0216058 and CHE-0407824 to J.A.P., CHE-0243951 to J.A.H., and CHE-0203346 to C.J.C.), the donors of the ACS Petroleum Research Fund (no. 37834-B6 to J.A.P.), and Research Corporation (no. CC5622 to J.A.P.). Additional support was provided by the Office of Research and Sponsored Programs at the University of Wisconsin−Eau Claire. Sabbatical support for J.A.P. was provided by the NSF-RSEC (CHE-0113894) program at the University of Minnesota.

Supporting Information Available: Crystallographic information files; calculated gas-phase frequencies and band intensities (Tables S1−S3). This material is available free of charge via the Internet at http://pubs.acs.org.

IC051491X